Distinct segregation patterns of yeast cell-peripheral proteins uncovered by a method for protein segregatome analysis

Shinju Sugiyama[a,b] and Motomasa Tanaka[a,b,1]

[a]Laboratory for Protein Conformation Diseases, RIKEN Center for Brain Science, Wako, 351-0198 Saitama, Japan; and [b]School of Life Science and Technology, Tokyo Institute of Technology, Yokohama, 226-8501 Kanagawa, Japan

Edited by John R. Pringle, Stanford University Medical Center, Stanford, CA, and approved March 21, 2019 (received for review November 22, 2018)

Protein segregation contributes to various cellular processes such as polarization, differentiation, and aging. However, the difficulty in global determination of protein segregation hampers our understanding of its mechanisms and physiological roles. Here, by developing a quantitative proteomics technique, we globally monitored segregation of preexisting and newly synthesized proteins during cell division of budding yeast, and identified crucial domains that determine the segregation of cell-peripheral proteins. Remarkably, the proteomic and subsequent microscopic analyses demonstrated that the flow through the bud neck of the proteins that harbor both endoplasmic reticulum (ER) membrane-spanning and plasma membrane (PM)-binding domains is not restricted by the previously suggested ER membrane or PM diffusion barriers but by septin-mediated partitioning of the PM-associated ER (pmaER). Furthermore, the proteomic analysis revealed that although the PM-spanning t-SNARE Sso2 was retained in mother cells, its paralog Sso1 unexpectedly showed symmetric localization. We found that the transport of Sso1 to buds was required for enhancement of polarized cell growth and resistance to cell-wall stress. Taken together, these data resolve long-standing questions about septin-mediated compartmentalization of the cell periphery, and provide new mechanistic insights into the segregation of cell-periphery proteins and their cellular functions.

asymmetric cell division | protein segregation | septin | ER–PM contact site | polarized cell growth

Various cellular components such as nucleic acids, proteins, lipids, and organelles are differentially distributed between mother cells and buds in yeast (1, 2). This asymmetric distribution creates cellular polarity and confers phenotypic differences, including stress resistance and cellular viability, between mother and daughter cells, suggesting that it contributes to maintenance of cellular homeostasis (1, 2). One of the major factors that cause asymmetric protein abundance between mother and daughter cells is uneven segregation of preexisting and newly synthesized proteins during cell division. For instance, since diffusion of plasma membrane (PM) transporters is slow due to their insertion into the PM, many preexisting transporters synthesized during previous cell cycles are retained in mother cells (3). An endoplasmic reticulum (ER)–PM contact-site protein, Ist2, was suggested to be exclusively distributed to mother cells due to ER membrane or PM diffusion barriers created by septins at the bud neck (4–6), although the identity of such diffusion barriers has remained obscure and it has been controversial which barrier is involved.

Due to the lack of a full catalog of symmetrically/asymmetrically segregated proteins, we have remarkably little knowledge about what and how proteins are segregated during cell division. Previous mass spectrometric and microscopic analyses identified several proteins that were asymmetrically retained in mother cells (7). However, the method in that study was designed to identify asymmetrically segregated, long-lived proteins that are stable over many cell cycles. In contrast, protein segregation propensity during a single cell cycle has remained unexplored at the whole-proteome level. To overcome this problem, we attempted to quantify the ratio of preexisting proteins to new proteins that were synthesized during the most recent cell cycle. We reasoned that it would be critical to fix yeast cells to prevent protein synthesis and degradation during cell harvesting and fractionation steps for precise quantification of protein abundance. Importantly, apart from the methodology, attempts to identify both symmetrically and asymmetrically segregated proteins have not been performed, which prevents us from identifying common features that determine symmetric or asymmetric segregation.

Here we developed a quantitative proteomics technique named "segregatome analysis" to globally investigate the segregation of preexisting and newly synthesized yeast proteins during a single cell division. This technique, including various optimized protocols with fixation of yeast cells, allowed us to compare, between mother and daughter cells, the ratio of the abundance of preexisting proteins to that of new proteins that were synthesized during the latest cell cycle. The expanded list of both symmetrically and asymmetrically segregated proteins together with systematic domain analysis identified crucial domains that determine protein segregation in the cell periphery. We found that both ER membrane-spanning and PM-binding domains are required for asymmetric segregation of ER–PM contact-site proteins, such as Ist2. Subsequent microscopic analyses revealed that

Significance

Protein segregation plays crucial roles in various cellular processes including morphogenesis, differentiation, and aging. However, due to technical limitations, it has been unclear what domains or structural elements determine symmetric or asymmetric protein distribution during cell division. Here, we developed a proteomics technique to comprehensively monitor protein segregation during a single cell division in budding yeast. Our systematic domain analyses and subsequent microscopic studies uncovered novel mechanisms and functions of protein segregation in the cell periphery. We surmise that protein segregation plays a crucial role in regulating various biological processes, such as polarized cell growth and cellular calcium flux, in larger eukaryotes.

Author contributions: S.S. and M.T. designed research; S.S. performed research; S.S. analyzed data; and S.S. and M.T. wrote the paper.

The authors declare no conflict of interest.

This article is a PNAS Direct Submission.

Data deposition: The raw mass spectrometric data described in this paper have been deposited in the ProteomeXchange Consortium, www.proteomexchange.org, via the Japan Proteome Standard Repository/Database (accession no. PXD012598).

[1]To whom correspondence should be addressed. Email: motomasa.tanaka@riken.jp.

This article contains supporting information online at www.pnas.org/lookup/suppl/doi:10.1073/pnas.1819715116/-/DCSupplemental.

Published online April 11, 2019.

septin-mediated partitioning of the PM-associated ER (pmaER) restricted the flow of those ER–PM contact-site proteins through the bud necks. Furthermore, although most PM-spanning proteins were retained in mother cells as previously suggested (3), the segregatome analysis revealed symmetric segregation of a target-soluble *N*-ethylmaleimide–sensitive factor attachment protein receptor (t-SNARE) protein, Sso1. We found that the transportation of Sso1 to buds is required for efficient polarized cell growth and resistance to cell-wall stress. The segregatome analysis in this study enhances our understanding of protein segregation in the cell periphery.

Results

Quantitative Segregatome Analysis in Yeast. To reveal mechanisms of protein segregation, we attempted to identify common features of symmetrically/asymmetrically segregated proteins. To this end, we sought to globally analyze the ratio of preexisting proteins to newly synthesized proteins during the most recent cell cycle in both mother and daughter cells (Fig. 1*A*). First, the cell cycle was arrested at G1 phase with the mating pheromone α-factor. Although the efficiency of synchronization by α-factor has been suggested to be low in synthetic media (8), we obtained satisfactory synchronization with an enrichment of nutrients and a longer pheromone treatment (*SI Appendix*, Fig. S1 *A* and *B*). Next, the arrested cells were stained with the fluorescent dye Cy5, to distinguish them from unlabeled daughter cells (9). After release from cell-cycle arrest, we labeled new proteins synthesized during the remaining cell cycle (S through M phases) with [^{13}C^{15}N]Lys and/or [^{13}C^{15}N]Arg by pulsed stable isotope labeling by amino acids in cell culture (pSILAC) (10). Then, the cells were fixed with methanol to terminate protein synthesis and degradation. After fixation, we sorted Cy5-positive mother cells and Cy5-negative daughter cells by flow cytometry (*SI Appendix*, Fig. S1*C*). The purity of daughter-enriched fractions was almost 100%, whereas that of mother-enriched fractions was ∼70%, due to a small fraction of unseparated cells (*SI Appendix*, Fig. S1 *C* and *D*). The proteins in each sorted fraction were digested and subjected to mass spectrometric analysis, and the ratio of preexisting proteins to newly synthesized proteins produced during the cell cycle was determined (Fig. 1*B* and Dataset S1). We detected 2,039 proteins that were in common between two independent experiments. We defined the asymmetry index as the difference of the preexisting protein ratio between mother-enriched and daughter-enriched fractions. Therefore, a high asymmetry index indicates the enrichment of preexisting proteins in mother cells and/or the enrichment of newly synthesized proteins in daughter cells. We detected 56 proteins that were in the top 5% of the asymmetry index (>0.097 in the first experiment and >0.129 in the second experiment; see *SI Appendix*, *Methods* for details) in both experiments (Fig. 1*C*).

The 56 proteins include 20 whose asymmetric segregation was previously observed in microscopic (3, 4, 7, 11) or proteomic analyses (12) (*SI Appendix*, Fig. S2*A*). In contrast, five proteins that were previously reported to be segregated asymmetrically (7, 12) showed a low asymmetry index in our analysis (*SI Appendix*, Fig. S2*A*). However, we found that the difference in segregation of these proteins could be explained by distinct culture conditions (see *SI Appendix*, *Text* and Fig. S2 *B–E* for details). Thus, our technique detected the previously known asymmetrically segregated proteins and further identified 36 novel candidates, substantially expanding the list of known asymmetrically segregated proteins (*SI Appendix*, Fig. S2*A*). Importantly, our dataset includes not only asymmetrically but also symmetrically segregated proteins, which enabled systematic comparison between the two populations.

Localization and Domain Analysis of Cell-Peripheral Proteins. Gene ontology analysis revealed that cell-peripheral proteins showed a high propensity for asymmetric segregation (Fig. 1*D*). To gain further insights into this result, we classified the cell-peripheral proteins into three groups based on subcellular localization: cell wall, PM-associated ER, and others (Fig. 1 *E–H*, brown, and Datasets S2, S3, and S4). From this analysis, we observed that most detected cell-wall proteins were in the top 5% of the asymmetry index (Fig. 1*E* and Dataset S2). This observation probably reflected their interactions with an immobile, mother-retained cell wall (13–15) and/or slow diffusion due to their insertion into the PM (3). Notably, six proteins annotated as cell-wall proteins (Mcd4, Ssa1, Ssa2, Tdh1, Tdh2, and Tdh3) were detected with low asymmetry indices. However, all of them have been reported to be mainly localized to the cytosol or ER (16, 17) (https://www.yeastgenome.org/). Thus, we concluded that all of the bona fide cell-wall proteins detected in this study were asymmetrically segregated.

Next, we examined cell-peripheral proteins that did not show localization either at the cell wall or pmaER but are presumably bound to or inserted into the PM (Fig. 1*G* and Dataset S4). We found that most of the asymmetrically segregated PM proteins have transmembrane domains (TMDs). This asymmetric segregation of PM-spanning proteins is consistent with previous reports that many transporters in the PM are retained in mother cells due to their slow diffusion (3). In contrast to the PM-spanning proteins, we found that except for the immobile Num1 (18), the majority of cell-peripheral proteins without TMDs were symmetrically segregated (Fig. 1*H*, *d* and *e*). This result was unexpected, as septins were previously reported to restrict diffusion of PM-bound proteins at the bud neck by creating PM diffusion barriers (4, 19). Thus, our results indicated that septins do not significantly restrict diffusion of most PM-bound proteins without TMDs.

Septin-Dependent Segregation of Preexisting ER–PM Contact-Site Proteins in Mother Cells. Intriguingly, several PM-binding proteins without PM-inserted TMDs were segregated asymmetrically (Fig. 1*H*, *b* and *e*). Among them, we focused on the four proteins (Ist2, Tcb1, Tcb2, and Tcb3) that are localized in the pmaER (Fig. 1*F* and Dataset S3). These proteins are characterized by the presence of both ER TMDs and PM-binding domains, and they play a critical role in the formation of ER–PM contact sites (20). The newly synthesized Ist2 in buds has been suggested to be prevented from entering mother cells by septin-dependent but poorly understood mechanisms (4). We thus examined whether the flow of preexisting Ist2 was also inhibited by septins by expressing green fluorescent protein (GFP)-fused Ist2 from an inducible *GAL1* promoter. After the shutdown of protein expression, preexisting GFP-Ist2 was exclusively localized to mother cells (Fig. 2*A*). Then, to examine whether this asymmetric localization depends on septins, we used the *cdc12-6* temperature-sensitive strain in which septins are disassembled (21). We found preexisting GFP-Ist2 to enter buds at the restrictive temperature in the *cdc12-6* strain (Fig. 2*A*). To confirm this result, we evaluated the flow of GFP-Ist2 from mother cells to buds by fluorescence recovery after photobleaching (FRAP). We specifically bleached the fluorescence in buds, and quantified the fluorescence recovery due to the flow of GFP-Ist2 from mother cells to buds. Since the fluorescence intensity of GFP-Ist2 in buds was low before photobleaching, its recovery rate does not represent an actual flow rate in principle. Therefore, to estimate how strongly the asymmetry of protein distribution is maintained, we calculated relative fluorescence intensities between buds and mother cells after photobleaching (bud-FRAP). The increase of relative GFP-Ist2 fluorescence was faster in *cdc12-6* cells than that in wild-type cells (Fig. 2 *B* and *C*). We further employed another yeast septin mutant, *shs1*Δ, in which the septin hourglass is partially disrupted (22), and observed a faster recovery of GFP-Ist2 fluorescence in *shs1*Δ buds as well (*SI Appendix*, Fig. S3*A*). These results together show that septins are responsible for the asymmetric distribution of preexisting

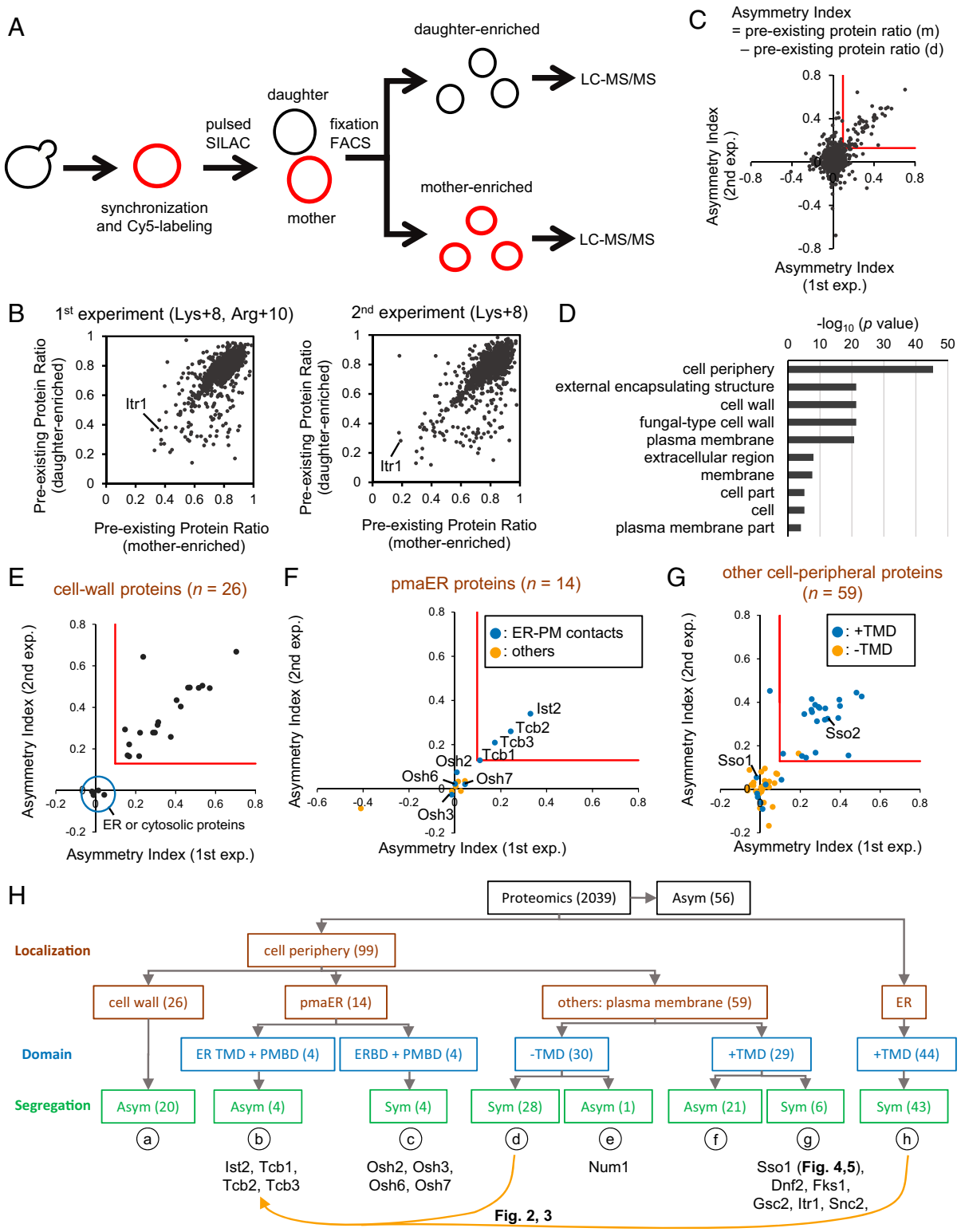

Fig. 1. Global analysis of protein segregation. (*A*) Experimental scheme of global analysis of protein segregation. (*B*) Plots of preexisting protein ratio (Dataset S1). (*C*) Plots of asymmetry index defined as the differences of the preexisting protein ratio between mother- and daughter-enriched fractions. Red lines indicate the top 5% of the asymmetry indices. (*D*) Top 10 gene ontology terms (cellular component) of asymmetrically segregated proteins. The 56 proteins that were in the top 5% of the asymmetry index in both experiments were subjected to this analysis. (*E*) Asymmetry indices of cell-wall proteins (gene ontology: fungal-type cell wall) (Dataset S2). Proteins in the blue circle were reported to be mainly localized to the ER or cytosol (see the main text). (*F*) Asymmetry indices of pmaER-localized proteins (gene ontology: cortical ER) (Dataset S3). (*G*) Asymmetry indices of cell-peripheral proteins (gene ontology: plasma membrane, cell periphery, or cell cortex) that are localized to neither the cell wall nor pmaER (Dataset S4). Only proteins confirmed to be localized to the cell periphery using fluorescence microscopy (16, 17) were plotted. Existence of transmembrane domains was predicted by TMHMM (65). (*H*) The flowchart of protein segregation in the cell periphery. Asym, asymmetric (asymmetry indices were greater than the top 5% thresholds in both experiments); Sym, symmetric (absolute values of asymmetry indices were equal to or less than the top 5% thresholds in both experiments). ERBD, ER-binding domain; PMBD, PM-binding domain.

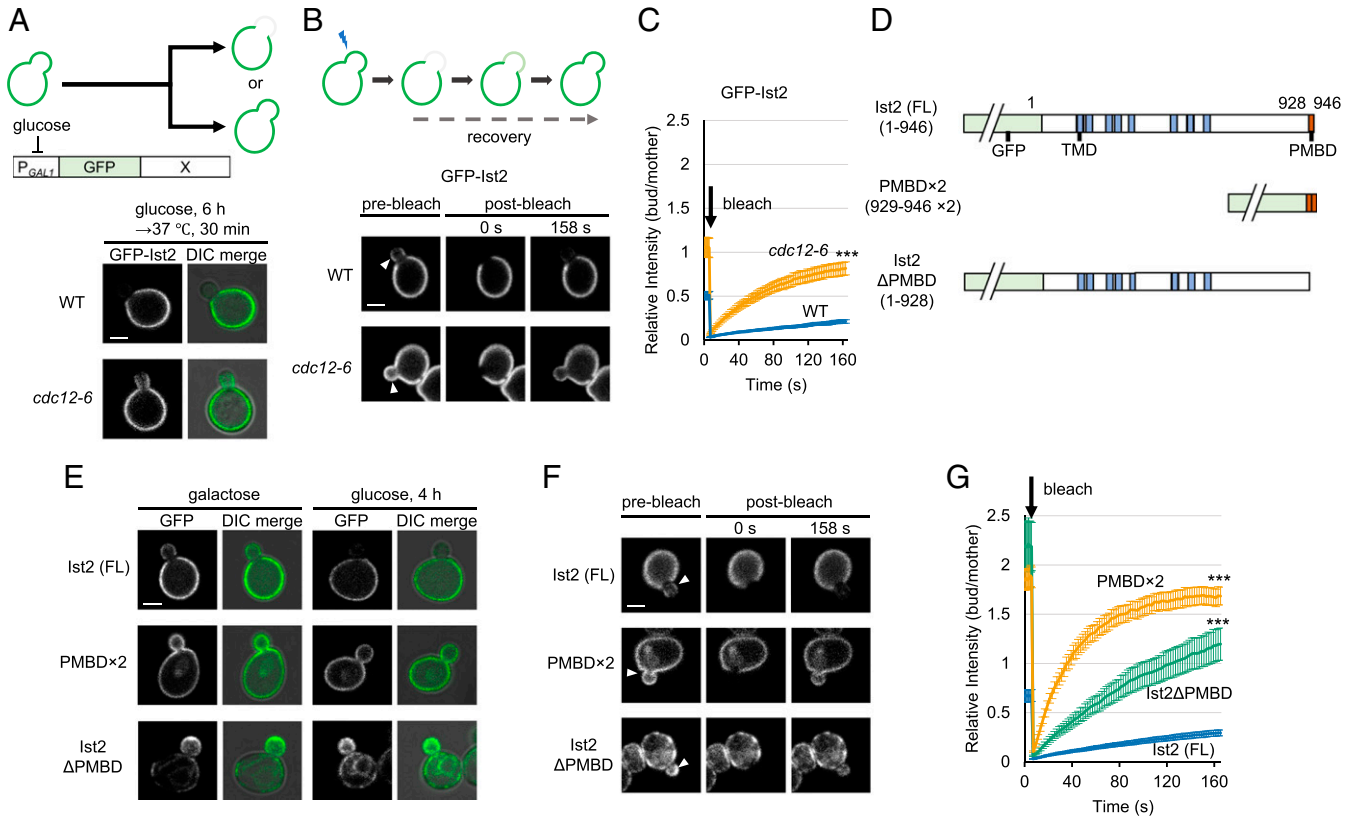

Fig. 2. Requirement for both the ER TMD and PM-binding domain for asymmetric segregation of ER–PM contact-site proteins. (*A*) Localization of preexisting GFP-Ist2 in wild-type or *cdc12-6*. GFP-Ist2 was expressed from the *GAL1* promoter. After transcriptional repression by adding glucose, cells were incubated at 23 °C for 6 h. Then, the cells were treated at 37 °C for 30 min. DIC, differential interference contrast. (Scale bar, 2 μm.) (*B* and *C*) Bud-FRAP of GFP-Ist2 in wild-type or *cdc12-6* buds (~1.5 μm). Cells were incubated at 37 °C for 30 min before the experiments. Arrowheads indicate bleached buds. (Scale bar, 2 μm.) Data are represented as means ± SEMs. $n = 15$. ***$P < 0.001$ (Welch's t test). (*D*) Structural domain diagrams of GFP-fused full-length (FL) and derivatives of Ist2. (*E*) Localization of preexisting Ist2 derivatives. GFP-fused proteins were expressed from the *GAL1* promoter. After addition of glucose, the cells were incubated for 4 h. (Scale bar, 2 μm.) (*F* and *G*) Bud-FRAP of Ist2-derived proteins. GFP in buds (~1.5 μm) was photobleached. (*F*) Arrowheads indicate bleached buds. (Scale bar, 2 μm.) (*G*) Data are represented as means ± SEMs. $n = 20$. ***$P < 0.001$ (Welch's t test with Bonferroni correction).

Ist2. Using this bud-FRAP method, we further investigated the flow of Tcb1, Tcb2, and Tcb3 from mother cells to buds. As observed for Ist2, the fluorescence recovery rates of Tcb1-GFP, Tcb2-GFP, and Tcb3-GFP were substantially faster in *cdc12-6* cells (*SI Appendix*, Fig. S3 *B–D*), indicating that the flow of these proteins is also restricted by septins. In contrast, the four proteins (Osh2, Osh3, Osh6, and Osh7) that are known to be localized to ER–PM contact sites by their lipid- or ER protein-binding domains (23) were symmetrically distributed (Fig. 1*F* and Dataset S3). In fact, fluorescence of these GFP-fused proteins was detected not only in the cell periphery but also in the cytoplasm (23) (*SI Appendix*, Fig. S3*E*). These results suggest that the binding of these four proteins to ER–PM contact sites is weak, and thereby these proteins can distribute freely between mother cells and buds through the cytosolic region at the bud neck. Taken together, these results established that septins restrict the flow of some of the proteins that are located at ER–PM contact sites.

Requirement of Both the ER TMD and PM-Binding Domain for Asymmetric Segregation of ER–PM Contact-Site Proteins. The septin complex at the bud neck was previously suggested to restrict the flow of both ER membrane proteins and PM-binding proteins by constituting diffusion barriers that have not yet been fully characterized (5, 19). However, our segregatome analysis surprisingly revealed the symmetric segregation of most ER membrane-spanning proteins and PM-binding proteins (Fig. 1 *G* and *H*, *SI Appendix*, Fig. S2*F*, and Datasets S4 and S5), suggesting that the asymmetric segregation of Ist2 cannot be explained solely either by its insertion into the ER membrane or by its binding to the PM. Moreover, as previously reported (5), the perturbation of ER compartmentalization by *BUD6* deletion did not affect the asymmetric segregation of Ist2 (*SI Appendix*, Fig. S3 *F* and *G*). In contrast, other ER compartmentalization-defective strains, the *scs2*Δ and *epo1*Δ mutants, were reported to show higher expression of Ist2 in buds than wild-type yeast (6). However, we found that preexisting Ist2 was still enriched in the mother cells of these deletion mutants (*SI Appendix*, Fig. S3 *F* and *G*). Thus, the impaired ER compartmentalization caused by deletion of *SCS2* or *EPO1* is likely to increase the abundance of newly synthesized Ist2 in buds rather than the protein flow from mother cells to buds. Furthermore, we confirmed that preexisting GFP-Ist2 was still enriched in mother cells lacking Sur2 (*SI Appendix*, Fig. S3 *F* and *G*), which is involved in sphingolipid synthesis and essential to intact ER compartmentalization (24). Taken together, these results indicate that the ER compartmentalization regulated by these nonseptin proteins is not involved in the asymmetric segregation of Ist2.

Next, we examined whether the binding of Ist2 to the PM is required for its asymmetric segregation. Ist2 has eight TMDs, which are inserted into the ER membrane, and one C-terminal polybasic domain that binds to the PM (20) (Fig. 2*D*). From the inducible *GAL1* promoter, we expressed a GFP-fused tandem repeat of the PM-binding domain derived from Ist2 (GFP-PMBD×2),

which strongly binds to the PM (20), and a truncated form of Ist2 lacking the PMBD (GFP-Ist2ΔPMBD). After the shutdown of protein expression, preexisting GFP-PMBD×2 and GFP-Ist2ΔPMBD were localized to both mother cells and buds (Fig. 2*E*). Using bud-FRAP, we found that both the mother-localized GFP-PMBD×2 and mother-localized GFP-Ist2ΔPMBD entered buds much faster than full-length GFP-Ist2 (Fig. 2 *F* and *G*). Thus, in Ist2, neither the PM-binding domain alone nor the TMDs alone are sufficient for the asymmetric segregation.

Next, we fused PMBD×2 of Ist2 to the symmetrically segregated ER transmembrane protein Sac1 (asymmetry index: 0.014 and 0.015), and examined the localization of the preexisting fusion protein. Sac1 itself does not have any PM-binding domains, an observation consistent with our finding that Sac1-GFP was localized to the whole ER including the nuclear envelope (*SI Appendix*, Fig. S3*H*). The fusion of Sac1 with the PMBD×2 sequence changed its localization to the cell periphery, indicating that Sac1-GFP-PMBD×2 had acquired the localization to ER–PM contact sites (*SI Appendix*, Fig. S3*H*). After the shutdown of protein expression, preexisting Sac1-GFP distributed in both mother cells and their buds, whereas preexisting Sac1-GFP-PMBD×2 was enriched in mother cells (*SI Appendix*, Fig. S3*H*). When septins were disrupted in *cdc12-6* yeast, preexisting Sac1-GFP-PMBD×2 entered buds (*SI Appendix*, Fig. S3 *I* and *J*). Taken together, the results indicate that both the ER TMDs and PM-binding domain are required for the septin-dependent asymmetric segregation of Ist2.

Septin-Mediated Partitioning of pmaER at the Bud Neck. To gain mechanistic insights into the septin-dependent restriction of protein flow at the bud neck, we focused on the distribution of Ist2. We found that full-length Ist2 was excluded from the bud neck, and this exclusion was lost in *cdc12-6* cells at the restrictive temperature (Figs. 2*B* and 3*B*). In contrast, GFP-PMBD×2 was continuously distributed through the bud neck (Fig. 2 *E* and *F*). Since Ist2 is a pmaER-localized protein, we hypothesized that septins partition the pmaER at the bud neck, and this partitioning prevents the flow of pmaER-localized proteins. To test this hypothesis, we first compared the morphology of the ER between wild-type and *cdc12-6* cells by fluorescence microscopy. We found that the ER lumen visualized by mCherry-HDEL showed a discontinuity at the bud neck, where septins are localized, in wild-type but not in *cdc12-6* cells (Fig. 3*A* and Movie S1). The ER at the bud neck of *cdc12-6* cells colocalized with GFP-Ist2, Tcb1-GFP, Tcb2-GFP, and Tcb3-GFP, indicating that the ER at the bud neck is indeed attached to the PM (Fig. 3 *B* and *C*, *SI Appendix*, Fig. S4 *A*–*C*, and Movie S2). Importantly, cytoplasmic ER, which was not bound to the PM, was continuous between mother cells and buds even in wild-type cells (Fig. 3*B*), which supports our hypothesis that pmaER, but not cytoplasmic ER, is disconnected by the septins. Similarly, in another yeast

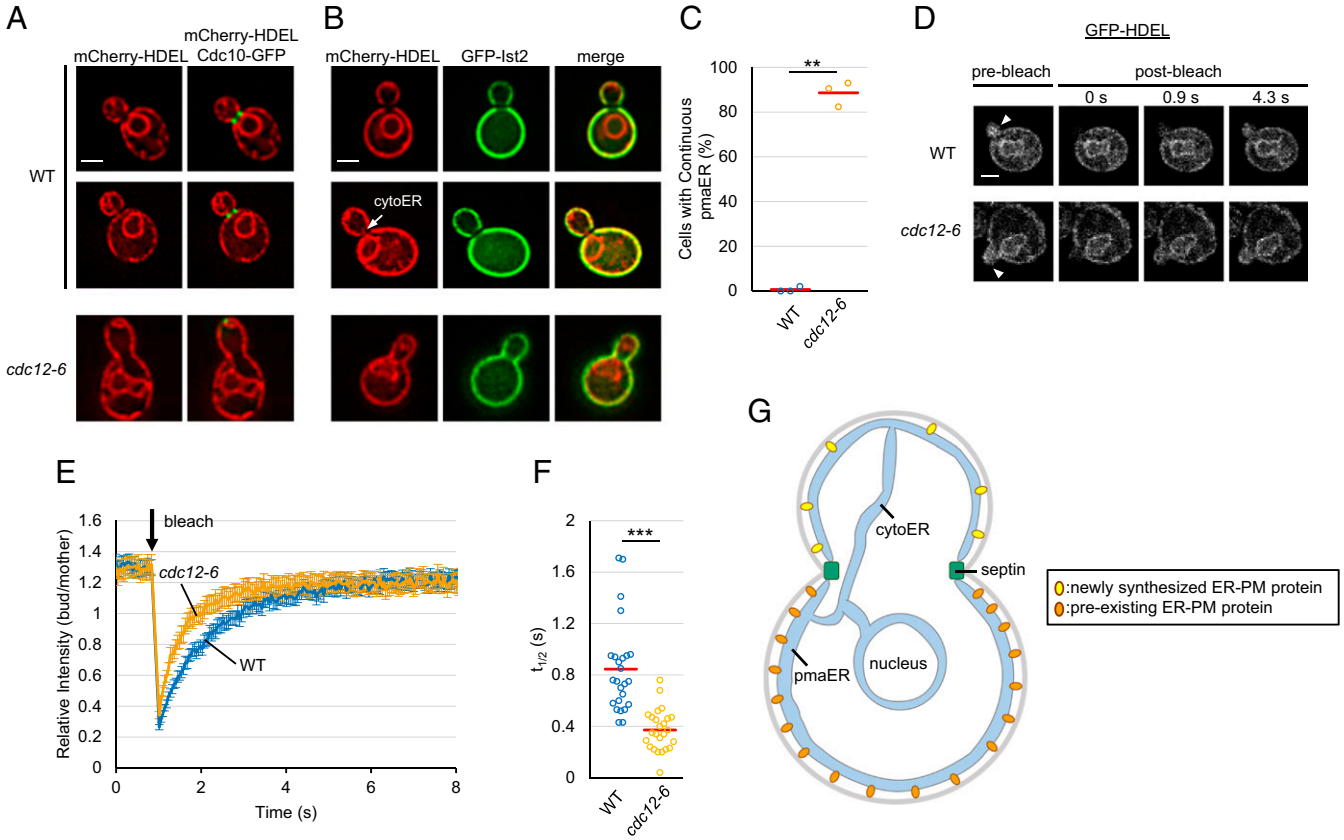

Fig. 3. Septin-mediated partitioning of the pmaER at the bud neck. (*A* and *B*) Representative images of the ER lumen (mCherry-HDEL) and septins (Cdc10-GFP) (*A*) or GFP-Ist2 (*B*) in wild-type (WT) or *cdc12-6* cells. Cells were incubated at the restrictive temperature (37 °C) for 30 min before imaging. The arrow indicates cytoplasmic ER (cytoER) at the bud neck. (Scale bars, 2 μm.) See also Movies S1 and S2. (*C*) Percentages of cells that have continuous ER colocalized with GFP-Ist2. Red bars represent means. ≥50 cells were examined in each experiment. $n = 3$. $^{**}P < 0.01$ (Welch's *t* test). (*D* and *E*) Bud-FRAP of GFP-HDEL in buds (~1.5 μm) of wild type and *cdc12-6*. Cells were incubated at 37 °C for 30 min before the experiments. Arrowheads indicate photobleached buds. (Scale bar, 2 μm.) Data are represented as means ± SEMs. $n = 25$. (*F*) Half-times of fluorescence recovery. Red bars indicate means. $^{***}P < 0.001$ (Welch's *t* test). (*G*) Model of septin-dependent restriction of ER protein flow. Septins partition the pmaER at the bud neck, and this partitioning blocks the flow of pmaER-localized proteins. Newly synthesized Ist2, Tcb2, and Tcb3 are enriched in buds by myosin-dependent mRNA transportation to the bud tip (4, 26).

septin mutant, *shs1*Δ, we observed continuous localization of Ist2-positive ER through the bud neck (*SI Appendix*, Fig. S4 *D–F*). These data suggest that septin-mediated partitioning of the pmaER at the bud neck is responsible for the asymmetric segregation of Ist2.

Septin-Restricted Flow of ER Lumen Proteins. A previous study investigated the flow of ER membrane and lumen proteins from mother cells to buds by photobleaching analysis (5). Since the flow of ER lumen proteins was much faster than that of ER membrane proteins, it was suggested that the flow of ER lumen proteins is not restricted by septins. Although this result might be taken to suggest the existence of membrane-specific diffusion barriers in the ER, it may not be conclusive, as the inherent diffusion rates of transmembrane proteins and lumen proteins are known to be substantially different (25). If septins partition the pmaER so that it becomes discontinuous at the bud neck, the flow of ER proteins between mother cells and buds is expected to be limited only to the pathways through the cytoplasmic ER and nuclear envelope. This situation will restrict the flow of ER lumen proteins at the bud neck. To examine whether septins indeed reduce the flow rate of ER lumen proteins, we examined the flow of GFP-HDEL from mother cells to buds by bud-FRAP. When buds were photobleached, the fluorescence recovery in *cdc12-6* cells was significantly faster than that in wild-type cells (Fig. 3 *D–F*). Similar results were obtained using the *shs1*Δ mutant (*SI Appendix*, Fig. S4 *G* and *H*). The observation that the flow of ER lumen proteins is also limited by septins supports our hypothesis that septin-mediated restriction of the ER protein flow is caused by the partitioning of the pmaER rather than the formation of ER membrane diffusion barriers (Fig. 3*G*).

Endocytic Recycling-Dependent Segregation of Sso1. Our segregatome analysis is useful not only for mechanistic investigation of protein segregation but also for identification of exceptional proteins that show segregation distinct from the majority of the proteins harboring similar domains (Fig. 1*H*, *e* and *g*). Although many PM-spanning proteins were segregated asymmetrically (Fig. 1*H*, *f*), presumably due to their slow diffusion (3), our segregatome analysis identified six exceptional PM-spanning proteins with low asymmetry indices (Dnf2, Fks1, Gsc2, Itr1, Snc2, and Sso1) (Fig. 1*H*, *g*). Among them, we focused on Sso1, since its paralog Sso2 was segregated asymmetrically (Fig. 1*G*), implying distinct biological roles.

Sso1 and Sso2 are both PM-spanning t-SNAREs and have a redundant function in membrane fusion during exocytosis (27). These proteins interact with other types of SNARE proteins in secretory vesicles and induce membrane fusion between vesicles and the PM. First, we examined the localizations of the newly synthesized proteins. Newly synthesized Sso1 and Sso2 were both enriched in the PM of buds (Fig. 4*A*), indicating that different localization of newly synthesized protein is not responsible for the difference in asymmetry index. After shutdown of protein expression, preexisting GFP-Sso1 was distributed symmetrically whereas GFP-Sso2 was enriched in mother cells (Fig. 4*B* and *SI Appendix*, Fig. S5*A*), consistent with our proteomics data. We found by bud-FRAP that the flow of GFP-Sso1 from mother cells to buds was much faster than that of GFP-Sso2 (Fig. 4 *C* and *D*). Despite the immobile nature of many PM-spanning

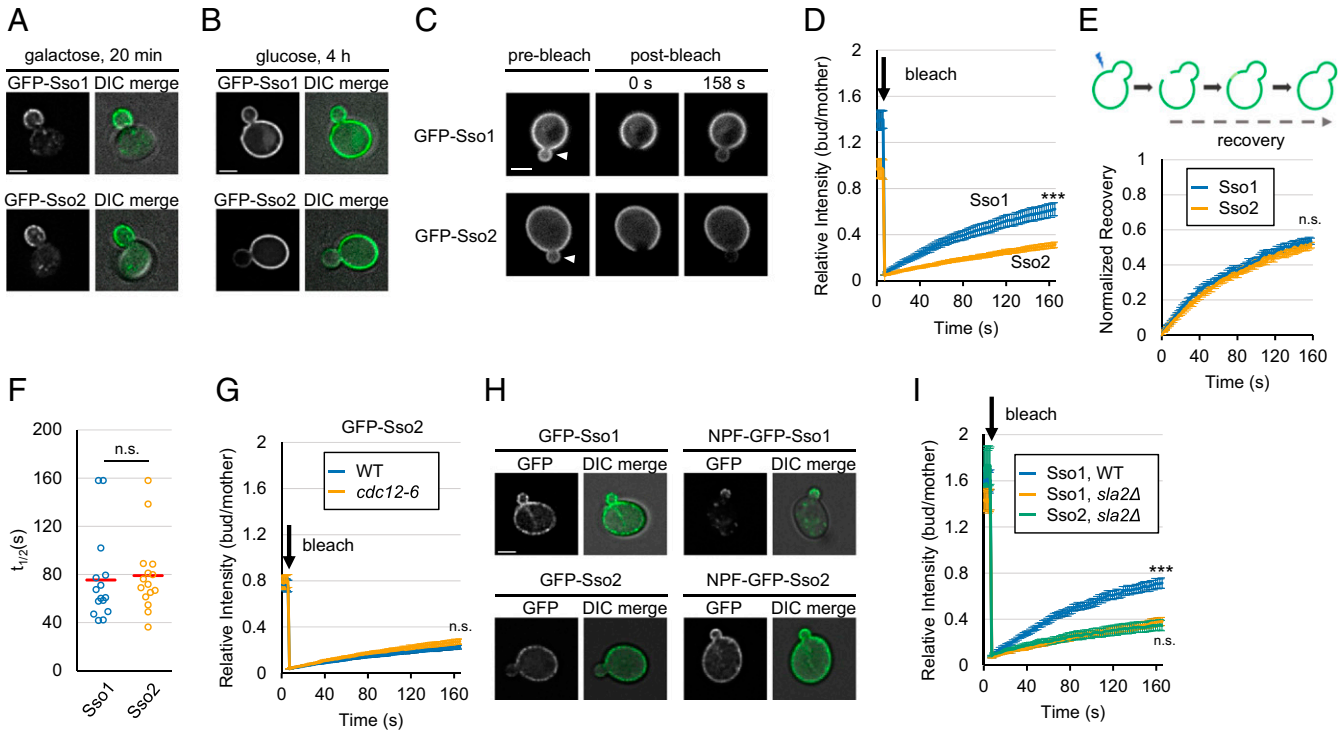

Fig. 4. Endocytic recycling-dependent transport of Sso1. (*A*) Localization of newly synthesized GFP-Sso1 or GFP-Sso2. Transcription of *GFP-SSO1* or *GFP-SSO2* was activated for 20 min. (Scale bar, 2 μm.) (*B*) Localization of preexisting GFP-Sso1 or GFP-Sso2. Transcription of *GFP-SSO1* or *GFP-SSO2* was repressed for 4 h. (Scale bar, 2 μm.) (*C* and *D*) Bud-FRAP of GFP-Sso1 and GFP-Sso2 (~1.5-μm buds). Arrowheads indicate photobleached buds. (Scale bar, 2 μm.) Data are represented as means ± SEMs. $n = 10$. ***$P < 0.001$ (Welch's *t* test). (*E*) Diffusion of GFP-Sso1 or GFP-Sso2. Data are represented as means ± SEMs. $n = 15$. n.s., not significant ($P > 0.05$ by Welch's *t* test). (*F*) Half-times of fluorescence recovery in *E*. Red bars indicate means. Not significant ($P > 0.05$ by Welch's *t* test). (*G*) Bud-FRAP of GFP-Sso2 in ~1.5-μm buds of *cdc12-6* cells. Cells were incubated at 37 °C for 30 min before the experiments. Data are represented as means ± SEMs. $n = 15$. Not significant ($P > 0.05$ by Welch's *t* test). (*H*) Localization of GFP-Sso1 or GFP-Sso2 fused with the endocytosis signal of Kex2 (NPF). (Scale bar, 2 μm.) (*I*) Bud-FRAP of GFP-Sso1 and GFP-Sso2 in *sla2*Δ cells (~1.5-μm buds). Data are represented as means ± SEMs. $n = 10$. Not significant ($P > 0.05$); ***$P <$ 0.001 (Welch's *t* test with Bonferroni correction). See also *SI Appendix*, Fig. S5*G*.

proteins, Sso1 was previously suggested to be diffusible in the PM (13). Thus, we compared the diffusion rate between GFP-Sso1 and GFP-Sso2 by FRAP; however, they showed similar fluorescence recovery rates (Fig. 4 *E* and *F*). Additionally, the asymmetric segregation of GFP-Sso2 was independent of septins (Fig. 4*G*). Furthermore, during bud-FRAP of GFP-Sso1, fluorescence at the bud tip was found to be recovered faster than that in the surroundings (*SI Appendix*, Fig. S5 *B–D*). These results suggested that preexisting Sso1 is transported to buds in a diffusion-independent manner.

A plant homolog of Sso1 and Sso2, SYP123, is endocytosed and transported to the sites of polarized cell growth (28). In yeast, a few PM-spanning proteins have been suggested to be transported to the PM in buds via endocytic recycling (13). Therefore, we examined whether GFP-Sso1 is a target of the recycling pathway. Because an endocytosis signal of Sso1 or an endocytosis-inhibitory signal of Sso2 has not yet been identified, we examined localization of the Sso proteins fused with an NPFXD endocytosis signal derived from Kex2 (29). GFP-Sso1 fused with the NPFXD signal (NPF-GFP-Sso1) was enriched in the PM of buds (13) (Fig. 4*H*). In contrast, NPF-GFP-Sso2 acquired PM localization in buds but showed localization in mother cells as well (Fig. 4*H*), suggesting that Sso1 is inherently more recycled. Furthermore, we found by bud-FRAP that inhibition of endocytosis by actin depolymerization (30) or loss of Sla2, an adaptor between clathrin and actin (31), significantly reduced the flow of GFP-Sso1 from mother cells to buds (Fig. 4*I* and *SI Appendix*, Fig. S5 *E–G*). This indicates that endocytosis is required for transport of preexisting GFP-Sso1 to buds. Taken together, our results suggest that symmetric distribution of Sso1 is caused by its endocytic recycling. Since GFP-Sso2 was not observed in internal vesicles or vacuoles (Fig. 4*H*), differences in susceptibility to endocytosis rather than that to recycling would appear to be responsible for retention of Sso2 in mother cells.

Enhanced Polarized Cell Growth and Resistance to Cell-Wall Stress by Endocytic Recycling of Sso1. The Sso homologs have been suggested to be required for efficient polarized cell growth in filamentous fungi, plants, and metazoans (28, 32, 33). Thus, we examined whether transport of preexisting Sso1 into buds has any impact on polarized cell growth. Some diploid *Saccharomyces cerevisiae* strains form elongated pseudohyphae under nitrogen-starvation conditions (34). As expected, homozygous *sso1*Δ cells show a rounder pseudohyphal morphology than wild-type and homozygous *sso2*Δ cells (Fig. 5*A*). Cell elongation of pseudohyphae occurs in the prolonged G2 phase (35). Therefore, to quantify bud elongation, we used the *cdc28-1N* mutant, which undergoes G2 arrest at the restrictive temperature (36). We found that *sso1*Δ cells formed less elongated buds during G2 arrest (Fig. 5 *B* and *C*). In elongated buds, GFP-Sso1 was

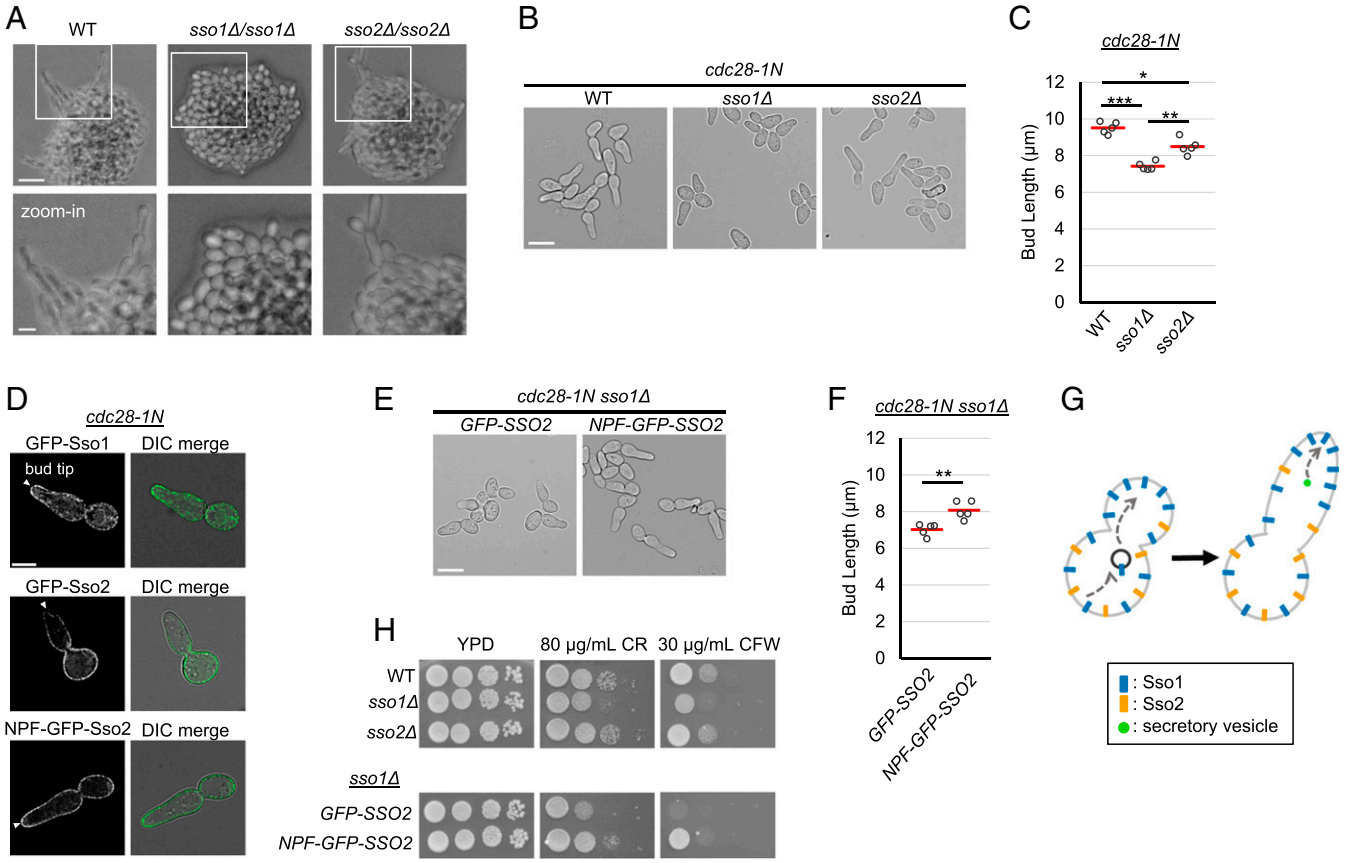

Fig. 5. Enhanced polarized cell growth and resistance to cell-wall stress by endocytic recycling of Sso1. (*A*) Pseudohyphae of homozygous diploids expressing functional Flo8, a transcription factor regulating pseudohyphal growth. Cells were grown on media with a low concentration of amino acids for 20 h. [Scale bars, 15 μm (*Top*) and 5 μm (*Bottom*).] (*B* and *C*) Bud elongation of G2-arrested cells. *cdc28-1N* cells were incubated at 37 °C for 3 h. (Scale bar, 10 μm.) ≥71 cells were examined in each measurement. $n = 5$. $^{*}P < 0.05$, $^{**}P < 0.01$, and $^{***}P < 0.001$ (Welch's *t* test with Bonferroni correction). (*D*) Localization of GFP-Sso1, GFP-Sso2, or NPF-GFP-Sso2 in elongated *cdc28-1N* cells. GFP-fused proteins were expressed from CEN/ARS plasmids in an *SSO1 SSO2* strain. Cells were incubated at 37 °C for 2.5 h. (Scale bar, 5 μm.) (*E* and *F*) Bud elongation of *sso1*Δ *cdc28-1N* cells expressing *GFP-SSO2* or *NPF-GFP-SSO2*. Cells were incubated at 37 °C for 3 h. (Scale bar, 10 μm.) ≥52 cells were examined in each measurement. $n = 5$. $^{**}P < 0.01$ (Welch's *t* test). (*G*) Model of cell-elongation enhancement by endocytic recycling of Sso1. (*H*) Resistance to Congo red (CR) or Calcofluor white (CFW). Cells were grown on the plates for 3 d.

localized to the bud tips whereas GFP-Sso2 was excluded (Fig. 5*D*). We then examined whether endocytosis of Sso proteins can enhance cell elongation. Remarkably, GFP-Sso2 with the NPFXD signal, which acquired localization at the bud tips (Fig. 5*D*), increased bud elongation (Fig. 5 *E* and *F*). These results indicate that endocytic recycling of Sso1 enhances polarized cell growth (Fig. 5*G*).

During cell division, the cell wall in buds is known to be highly remodeled (14). Since Sso1 shows localization in buds, we examined the effects of Sso1 endocytosis on cell-wall integrity. As previously reported (37), deletion of *SSO1* resulted in an increase in the sensitivity to Congo red, which binds to chitin and alters cell-wall structures (Fig. 5*H*). In contrast, such sensitivity was not observed in *sso2*Δ cells. Similar results were obtained with another cell-wall stressor, Calcofluor white (Fig. 5*H*). Importantly, we found that the introduction of the NPFXD signal that enhanced endocytosis of GFP-Sso2 also increased the resistance to both Congo red and Calcofluor white (Fig. 5*H*). These results suggest that endocytosis of Sso1 confers the cells with resistance to cell-wall stressors by enhanced localization to buds.

Discussion

Development of the Segregatome Technique. In this study, the segregatome technique globally identified both symmetrically and asymmetrically segregated proteins during a single cell division. Since we fixed cells before cell sorting, we excluded the effect of mother- or daughter-specific protein synthesis and degradation after cytokinesis. Importantly, we identified previously reported asymmetrically segregated proteins in addition to many novel candidates. Furthermore, by lowering thresholds, we could detect additional proteins previously identified as asymmetrically segregated, such as Asp1 (*SI Appendix*, *Text* and Fig. S2*B*) (12) and Kin4 (asymmetry indices: 0.079 and 0.073) (38), whose segregation is partially asymmetric due to their localization to multiple places. Taken together, these results validated our technique and suggest that the 30% of unseparated cells did not substantially affect our proteomic analysis, although this limitation may also be addressed by further studies.

It should be noted that protein segregation can be affected by various environmental and cellular factors including not only protein synthesis, degradation, and transportation (Fig. 4 and *SI Appendix*, Fig. S2*C*) but also posttranslational protein modification (39) and the lipid composition of the PM (40). Additionally, a range of protein aggregates that are formed by cellular stress or aging tend to be retained in mother cells (7, 41). Such protein aggregates could sequester preexisting proteins and alter the mode of protein segregation during cell division (7). The proteomics technique developed in this study will be readily applicable to cells under various conditions or environments. Therefore, this methodology will provide a versatile means to investigate condition-dependent protein segregatome during cell division and its physiological or pathological impact on cellular homeostasis.

Asymmetric Segregation of ER–PM Contact-Site Proteins. Protein segregatome analysis has resolved long-standing, puzzling questions about the asymmetric segregation of ER–PM contact-site proteins (4, 12). Septins were previously reported to restrict the movement of ER membrane or PM proteins through the bud neck by creating ER membrane or PM diffusion barriers, respectively (4, 5, 19). However, it has remained unclear what molecules constitute such diffusion barriers, how septins create both ER membrane and PM diffusion barriers with only their single membrane-binding domains, and whether this diffusion-barrier model can fully explain the asymmetric distribution of ER–PM contact-site proteins. By proteomic analysis, we found unexpectedly that the majority of ER transmembrane proteins and PM-binding proteins were symmetrically segregated (Fig. 1*H*, *d* and *h*), implying that ER membrane and PM diffusion barriers do not significantly restrict diffusion of ER and PM proteins, respectively. Therefore, the asymmetric segregation of ER–PM contact-site proteins such as Ist2 cannot be explained simply by either ER membrane or PM diffusion barriers. Instead, we found that septins partition the pmaER at the bud neck, which restricts the flow of ER-localized proteins, especially ER–PM contact-site proteins (Fig. 3*G*). Since septins attach to the phosphoinositide of the PM via their polybasic domains (42), we surmise that the PM-bound large septin complex structure prevents extension of the pmaER beyond the bud neck, resulting in pmaER partitioning at this location. Consistent with this interpretation, we found that septins restrict the flow of ER lumen proteins as well as ER membrane proteins (Fig. 3 *D*–*F*), even though the ER membrane diffusion-barrier model assumed that the flow of ER lumen proteins is not restricted by septins (5). Furthermore, our model is supported by the observation by electron microscopy that the pmaER, but not cytoplasmic ER, is excluded from the bud neck (43). The septin-mediated pmaER-partitioning model reconciles these previously contradictory observations.

ER–PM contact-site proteins are known to regulate various biological processes including assembly of the actomyosin ring, lipid composition at the PM, and calcium influx (44, 45). Thus, septin-dependent spatial regulation of ER–PM contact sites may be critical to modulate these cellular processes. For example, septins in metazoans regulate, via an as-yet unknown mechanism (46), the interaction between STIM1 and ORAI1, a PM calcium channel, which enables calcium entry upon activation (47). Since STIM1 contains both the ER TMD and PM-binding domains, our study predicts that septin-dependent restriction of STIM1's localization likely regulates the interaction with ORAI1 and thereby intracellular calcium concentration. Notably, septins are often located at the transition zones between distinct cellular compartments, such as the spine neck of neuronal dendrites and the base of primary cilia (48). Junctophilin, a protein family localized to ER–PM contact sites, has been suggested to regulate neuronal activity by controlling the functional communication between an ER-localized ryanodine receptor, a PM-localized *N*-methyl-D-aspartate receptor, and a Ca^{2+}-dependent K^+ channel, leading to memory formation (49). Therefore, septin-dependent distribution of junctophilin at spine necks may regulate this cascade and synaptic plasticity.

Segregation of PM Proteins. Septins were previously suggested to restrict diffusion of PM-binding proteins at the bud necks, as bud- or bud neck-enriched localization of several PM-associating proteins was diminished in septin mutants (19, 50). However, we found symmetric segregation of the majority of the PM-binding proteins (Fig. 1*H*, *d*) and PM-binding domains of Ist2 (Fig. 2 *E*–*G*). Therefore, PM diffusion barriers may have selectivity or exist only at specific stages of the cell cycle that determine particular complex septin structures (51). Additionally, as previously noted (52–54), other functions of septins may be responsible for the bud- or bud neck-enriched localization of PM-associating proteins.

Although many PM-spanning proteins are segregated asymmetrically due to their slow diffusion (3), our segregatome analysis identified several proteins that showed unusual segregation (Fig. 1*H*, *e* and *g*). In particular, we found that preexisting Sso1, but not Sso2, is transported to buds via endocytic recycling, which enhanced cell elongation (Fig. 5*G*). During pseudohyphal growth under nitrogen-starvation conditions, cells elongate and intrude into solid media, which helps them to search for and reach nutrient-rich environments (34). Since protein synthesis is substantially reduced under nitrogen-starvation conditions (55), it is likely that endocytic recycling of Sso1 can increase protein abundance at the bud tip more efficiently than enhancement of new protein synthesis. Importantly, pseudohyphal growth has been suggested to be required for the virulence of pathogenic

yeast strains (56). Thus, the transport of Sso1 may be crucial for the pathogenesis of *S. cerevisiae*. Furthermore, previous studies in metazoans and plants suggested the endocytosis-mediated relocalization of Sso homologs to the sites of polarized cell growth (28, 57), indicating an evolutionarily conserved role in polarized cell growth.

Finally, we identified five additional PM-spanning proteins that unexpectedly segregated symmetrically (Fig. 1*H*, *g*). One of them, Itr1, was endocytosed to the vacuole under our growth conditions (*SI Appendix*, *Text* and Fig. S2*C*), suggesting that the susceptibility of Itr1 to endocytic degradation is responsible for its low asymmetry index. The other four proteins (Dnf2, Fks1, Gsc2, and Snc2) were reported to be enriched in buds (16, 17), which implies their endocytic recycling-mediated transport to the buds. While secretory vesicles are transported to buds in the early stages of the cell cycle, these vesicles are enriched at the bud neck just before and during cytokinesis (58). Therefore, those four proteins would be symmetrically distributed between the former bud necks of divided cells after cytokinesis. Indeed, unlike nonpolarized GFP-Sso1 (*SI Appendix*, Fig. S5*A*), Fks1 was reported to be enriched at the bud neck during and after cytokinesis (59). Thus, we surmise that the four proteins are symmetrically distributed via the endocytic recycling-mediated transport to the bud neck. Since those four proteins play roles in cellular polarization, cell-wall synthesis, or exocytosis (60–62), we speculate that their transport also regulates polarized cell growth and/or resistance to cell-wall stress.

In summary, we classified the segregation of preexisting and newly synthesized proteins in the cell periphery and revealed novel mechanisms and functions. These findings provide new insights into protein segregation and cellular compartmentalization in the cell periphery. Further analyses of the dataset constructed in this study and expansion of the list for symmetrically/asymmetrically segregated proteins should deepen our understanding of the mechanisms and functions of protein segregation.

Methods

Yeast Strains, Growth Conditions, and Plasmids. Yeast strains and plasmids used in this study are listed in *SI Appendix*, Tables S1 and S2, respectively. Yeast cells were grown at 30 °C unless otherwise noted. Additional experimental details are provided in *SI Appendix*, *Methods*.

Synchronization, pSILAC, and Cell Sorting. Cells were grown in 25 mL of synthetic glucose medium with light lysine and arginine. At OD 0.7 to 0.8, the cells were washed with fresh medium and resuspended in the same amount of the medium. Then, the yeasts were treated with 10 μM α-factor (Zymo Research) for 6 h. After washing with PBS, the cells were resuspended in 50 μL of PBS. One-fifth of a vial of Cy5 postlabeling reactive dye pack (GE Healthcare) dissolved in 200 μL of PBS was added to the cell suspension. After a 5-min incubation, the labeled cells were washed with synthetic medium containing stable isotope-labeled [$^{13}C_6{}^{15}N_2$]Lys_2HCl and/or [$^{13}C_6{}^{15}N_4$]ArgHCl (Cambridge Isotope Laboratories), and then the cells were resuspended in 25 mL of the same medium. After incubation at 30 °C for 90 min, the cells were collected on Ultrafree-MC, HV, 0.45-μm filter units (Merck Millipore) by centrifugation at 1,000 × *g* for 1 min. The cells on the filters were fixed with methanol at −30 °C for 1 h, 4 °C for 30 min, and 30 °C for 15 min. Then, the fixed cells were resuspended in PBS and briefly sonicated to separate mother and daughter cells. Cy5-positive mother cells and Cy5-negative daughter cells were sorted with a FACSAria II SORP (BD). Proteins of the sorted cells were digested by the filter-aided sample preparation (FASP) method (63). Then, the digested peptides were desalted and fractionated into six fractions with C18 (3M) stage tips and SCX (3M) stage tips (64). The fractionated peptides were applied to a liquid chromatograph (LC) (EASY-nLC 1000; Thermo Fisher Scientific) coupled to a Q Exactive Hybrid Quadrupole-Orbitrap mass spectrometer (Thermo Fisher Scientific). Additional experimental details are provided in *SI Appendix*, *Methods*.

Microscopy. For microscopic observation, cells were mounted on Con A (Nacalai Tesque)-coated coverslips and visualized with a TCS SP8 (Leica Microsystems) or Personal Delta Vision (GE Healthcare) microscope. The TCS SP8 was equipped with an HC PL APO 63×/1.40 oil CS2 objective lens. GFP was excited by a 488-nm optically pumped semiconductor laser, and fluorescence in a range between 495 and 550 nm was detected with HyD detectors. Acquired images were processed with Las X software (Leica Microsystems). The Personal Delta Vision was equipped with a UPlanApo 20×/0.70 (Olympus) or PLAPON 60XO N.A. 1.42 objective lens (Olympus) and pco.edge 5.5 sCMOS sensor (PCO). GFP fluorescence was detected using an excitation filter of 475/28 nm and an emission filter of 525/48 nm. To detect mCherry fluorescence, an excitation filter of 575/25 nm and an emission filter of 625/45 nm were used. Cy5 was excited using a 632/22-nm filter, and its fluorescence passing through a 679/34-nm filter was detected. z-stack images were acquired every 0.15 μm. Acquired images were processed and deconvolved using Soft WoRx version 6.1.3 (GE Healthcare). Additional experimental details are provided in *SI Appendix*, *Methods*.

Statistical Analysis. Statistical significance was assessed by using two-tailed Welch's *t* test with Excel 2016. Bonferroni correction was used for multiple comparison. $*P < 0.05$, $**P < 0.01$, and $***P < 0.001$ were considered to be statistically significant.

Data Availability. The raw mass spectrometric data were deposited in the ProteomeXchange (accession no. PXD012598) via the Japan Proteome Standard Repository/Database (66).

ACKNOWLEDGMENTS. We thank Dr. Michael Knop for providing plasmids; Dr. Takehiko Itoh for encouragement; Dr. Amanda Alvarez, Kelvin Hui, and Marek Krzyzanowski for critical reading of the manuscript; and Naomi Takahashi for preparation of culture media and purification of plasmids. DNA sequencing, FACS, and mass spectrometry were performed by the RIKEN Center for Brain Science Research Resources Division. This work was supported by JSPS Research Fellowships for Young Scientists (Grant DC1, 16J07398 to S.S.), RIKEN Pioneering Projects Cellular Evolution (M.T.), Grant-in-Aid for Scientific Research on Innovative Areas (26116004 to M.T.), and RIKEN Aging Project (M.T.).

1. Higuchi-Sanabria R, et al. (2014) Role of asymmetric cell division in lifespan control in *Saccharomyces cerevisiae*. *FEMS Yeast Res* 14:1133–1146.
2. Martin SG, Arkowitz RA (2014) Cell polarization in budding and fission yeasts. *FEMS Microbiol Rev* 38:228–253.
3. Eldakak A, et al. (2010) Asymmetrically inherited multidrug resistance transporters are recessive determinants in cellular replicative ageing. *Nat Cell Biol* 12:799–805.
4. Takizawa PA, DeRisi JL, Wilhelm JE, Vale RD (2000) Plasma membrane compartmentalization in yeast by messenger RNA transport and a septin diffusion barrier. *Science* 290:341–344.
5. Luedeke C, et al. (2005) Septin-dependent compartmentalization of the endoplasmic reticulum during yeast polarized growth. *J Cell Biol* 169:897–908.
6. Chao JT, et al. (2014) Polarization of the endoplasmic reticulum by ER-septin tethering. *Cell* 158:620–632.
7. Thayer NH, et al. (2014) Identification of long-lived proteins retained in cells undergoing repeated asymmetric divisions. *Proc Natl Acad Sci USA* 111:14019–14026.
8. Juanes MA (2017) Methods of synchronization of yeast cells for the analysis of cell cycle progression. *Methods Mol Biol* 1505:19–34.
9. Chin CS, Chubukov V, Jolly ER, DeRisi J, Li H (2008) Dynamics and design principles of a basic regulatory architecture controlling metabolic pathways. *PLoS Biol* 6:e146.
10. Schwanhäusser B, Gossen M, Dittmar G, Selbach M (2009) Global analysis of cellular protein translation by pulsed SILAC. *Proteomics* 9:205–209.
11. Khmelinskii A, et al. (2012) Tandem fluorescent protein timers for in vivo analysis of protein dynamics. *Nat Biotechnol* 30:708–714.
12. Okada M, Kusunoki S, Ishibashi Y, Kito K (2017) Proteomics analysis for asymmetric inheritance of preexisting proteins between mother and daughter cells in budding yeast. *Genes Cells* 22:591–601.
13. Valdez-Taubas J, Pelham HRB (2003) Slow diffusion of proteins in the yeast plasma membrane allows polarity to be maintained by endocytic cycling. *Curr Biol* 13:1636–1640.
14. Johnson BF, Gibson EJ (1966) Autoradiographic analysis of regional cell wall growth of yeasts. III. *Saccharomyces cerevisiae*. *Exp Cell Res* 41:580–591.
15. Farkas V, Kovarík J, Kosinová A, Bauer S (1974) Autoradiographic study of mannan incorporation into the growing cell walls of *Saccharomyces cerevisiae*. *J Bacteriol* 117:265–269.
16. Huh WK, et al. (2003) Global analysis of protein localization in budding yeast. *Nature* 425:686–691.
17. Weill U, et al. (2018) Genome-wide SWAp-Tag yeast libraries for proteome exploration. *Nat Methods* 15:617–622.
18. Omer S, Greenberg SR, Lee W-L (2018) Cortical dynein pulling mechanism is regulated by differentially targeted attachment molecule Num1. *eLife* 7:e36745.
19. Barral Y, Mermall V, Mooseker MS, Snyder M (2000) Compartmentalization of the cell cortex by septins is required for maintenance of cell polarity in yeast. *Mol Cell* 5:841–851.

20. Manford AG, Stefan CJ, Yuan HL, Macgurn JA, Emr SD (2012) ER-to-plasma membrane tethering proteins regulate cell signaling and ER morphology. *Dev Cell* 23:1129–1140.
21. Haarer BK, Pringle JR (1987) Immunofluorescence localization of the *Saccharomyces cerevisiae CDC12* gene product to the vicinity of the 10-nm filaments in the mother-bud neck. *Mol Cell Biol* 7:3678–3687.
22. Garcia G, III, et al. (2011) Subunit-dependent modulation of septin assembly: Budding yeast septin Shs1 promotes ring and gauze formation. *J Cell Biol* 195:993–1004.
23. Schulz TA, et al. (2009) Lipid-regulated sterol transfer between closely apposed membranes by oxysterol-binding protein homologues. *J Cell Biol* 187:889–903.
24. Clay L, et al. (2014) A sphingolipid-dependent diffusion barrier confines ER stress to the yeast mother cell. *eLife* 3:e01883.
25. Levin MH, Haggie PM, Vetrivel L, Verkman AS (2001) Diffusion in the endoplasmic reticulum of an aquaporin-2 mutant causing human nephrogenic diabetes insipidus. *J Biol Chem* 276:21331–21336.
26. Shepard KA, et al. (2003) Widespread cytoplasmic mRNA transport in yeast: Identification of 22 bud-localized transcripts using DNA microarray analysis. *Proc Natl Acad Sci USA* 100:11429–11434.
27. Aalto MK, Ronne H, Keränen S (1993) Yeast syntaxins Sso1p and Sso2p belong to a family of related membrane proteins that function in vesicular transport. *EMBO J* 12: 4095–4104.
28. Ichikawa M, et al. (2014) Syntaxin of plant proteins SYP123 and SYP132 mediate root hair tip growth in *Arabidopsis thaliana*. *Plant Cell Physiol* 55:790–800.
29. Tan PK, Howard JP, Payne GS (1996) The sequence NPFXD defines a new class of endocytosis signal in *Saccharomyces cerevisiae*. *J Cell Biol* 135:1789–1800.
30. Ayscough KR, et al. (1997) High rates of actin filament turnover in budding yeast and roles for actin in establishment and maintenance of cell polarity revealed using the actin inhibitor latrunculin-A. *J Cell Biol* 137:399–416.
31. Wesp A, et al. (1997) End4p/Sla2p interacts with actin-associated proteins for endocytosis in *Saccharomyces cerevisiae*. *Mol Biol Cell* 8:2291–2306.
32. Bernardo SM, Rane HS, Chavez-Dozal A, Lee SA (2014) Secretion and filamentation are mediated by the *Candida albicans* t-SNAREs Sso2p and Sec9p. *FEMS Yeast Res* 14: 762–775.
33. Soo Hoo L, et al. (2016) The SNARE protein syntaxin 3 confers specificity for polarized axonal trafficking in neurons. *PLoS One* 11:e0163671.
34. Gimeno CJ, Ljungdahl PO, Styles CA, Fink GR (1992) Unipolar cell divisions in the yeast *S. cerevisiae* lead to filamentous growth: Regulation by starvation and RAS. *Cell* 68: 1077–1090.
35. Kron SJ, Styles CA, Fink GR (1994) Symmetric cell division in pseudohyphae of the yeast *Saccharomyces cerevisiae*. *Mol Biol Cell* 5:1003–1022.
36. Surana U, et al. (1991) The role of *CDC28* and cyclins during mitosis in the budding yeast *S. cerevisiae*. *Cell* 65:145–161.
37. García R, et al. (2015) Genomic profiling of fungal cell wall-interfering compounds: Identification of a common gene signature. *BMC Genomics* 16:683.
38. D'Aquino KE, et al. (2005) The protein kinase Kin4 inhibits exit from mitosis in response to spindle position defects. *Mol Cell* 19:223–234.
39. Xu P, et al. (2017) COPI mediates recycling of an exocytic SNARE by recognition of a ubiquitin sorting signal. *eLife* 6:e28342.
40. Singh P, et al. (2017) Sphingolipids facilitate age asymmetry of membrane proteins in dividing yeast cells. *Mol Biol Cell* 28:2712–2722.
41. Schneider KL, Nyström T, Widlund PO (2018) Studying spatial protein quality control, proteopathies, and aging using different model misfolding proteins in *S. cerevisiae*. *Front Mol Neurosci* 11:249.
42. Zhang J, et al. (1999) Phosphatidylinositol polyphosphate binding to the mammalian septin H5 is modulated by GTP. *Curr Biol* 9:1458–1467.
43. West M, Zurek N, Hoenger A, Voeltz GK (2011) A 3D analysis of yeast ER structure reveals how ER domains are organized by membrane curvature. *J Cell Biol* 193: 333–346.
44. Saheki Y, De Camilli P (2017) Endoplasmic reticulum–plasma membrane contact sites. *Annu Rev Biochem* 86:659–684.
45. Zhang D, Bidone TC, Vavylonis D (2016) ER-PM contacts define actomyosin kinetics for proper contractile ring assembly. *Curr Biol* 26:647–653.
46. Deb BK, Hasan G (2016) Regulation of store-operated Ca^{2+} entry by septins. *Front Cell Dev Biol* 4:142.
47. Sharma S, et al. (2013) An siRNA screen for NFAT activation identifies septins as coordinators of store-operated Ca^{2+} entry. *Nature* 499:238–242.
48. Saarikangas J, Barral Y (2011) The emerging functions of septins in metazoans. *EMBO Rep* 12:1118–1126.
49. Moriguchi S, et al. (2006) Functional uncoupling between Ca^{2+} release and afterhyperpolarization in mutant hippocampal neurons lacking junctophilins. *Proc Natl Acad Sci USA* 103:10811–10816.
50. Dobbelaere J, Barral Y (2004) Spatial coordination of cytokinetic events by compartmentalization of the cell cortex. *Science* 305:393–396.
51. Glomb O, Gronemeyer T (2016) Septin organization and functions in budding yeast. *Front Cell Dev Biol* 4:123.
52. Trimble WS, Grinstein S (2015) Barriers to the free diffusion of proteins and lipids in the plasma membrane. *J Cell Biol* 208:259–271.
53. Caudron F, Barral Y (2009) Septins and the lateral compartmentalization of eukaryotic membranes. *Dev Cell* 16:493–506.
54. Wloka C, et al. (2011) Evidence that a septin diffusion barrier is dispensable for cytokinesis in budding yeast. *Biol Chem* 392:813–829.
55. Kelly SP, Bedwell DM (2015) Both the autophagy and proteasomal pathways facilitate the Ubp3p-dependent depletion of a subset of translation and RNA turnover factors during nitrogen starvation in *Saccharomyces cerevisiae*. *RNA* 21:898–910.
56. McCusker JH, Clemons KV, Stevens DA, Davis RW (1994) *Saccharomyces cerevisiae* virulence phenotype as determined with CD-1 mice is associated with the ability to grow at 42 degrees C and form pseudohyphae. *Infect Immun* 62:5447–5455.
57. Sharma N, Low SH, Misra S, Pallavi B, Weimbs T (2006) Apical targeting of syntaxin 3 is essential for epithelial cell polarity. *J Cell Biol* 173:937–948.
58. Bi E, Park HO (2012) Cell polarization and cytokinesis in budding yeast. *Genetics* 191: 347–387.
59. Onishi M, Ko N, Nishihama R, Pringle JR (2013) Distinct roles of Rho1, Cdc42, and Cyk3 in septum formation and abscission during yeast cytokinesis. *J Cell Biol* 202: 311–329.
60. Burri L, Lithgow T (2004) A complete set of SNAREs in yeast. *Traffic* 5:45–52.
61. Das A, et al. (2012) Flippase-mediated phospholipid asymmetry promotes fast Cdc42 recycling in dynamic maintenance of cell polarity. *Nat Cell Biol* 14:304–310.
62. Inoue SB, et al. (1995) Characterization and gene cloning of 1,3-β-D-glucan synthase from *Saccharomyces cerevisiae*. *Eur J Biochem* 231:845–854.
63. Wiśniewski JR, Zougman A, Nagaraj N, Mann M (2009) Universal sample preparation method for proteome analysis. *Nat Methods* 6:359–362.
64. Rappsilber J, Ishihama Y, Mann M (2003) Stop and go extraction tips for matrix-assisted laser desorption/ionization, nanoelectrospray, and LC/MS sample pretreatment in proteomics. *Anal Chem* 75:663–670.
65. Krogh A, Larsson B, von Heijne G, Sonnhammer EL (2001) Predicting transmembrane protein topology with a hidden Markov model: Application to complete genomes. *J Mol Biol* 305:567–580.
66. Sugiyama S, Tanaka M (2019) Protein segregation in budding yeast. ProteomeXchange. Available at proteomecentral.proteomexchange.org/cgi/GetDataset?ID=PXD012598. Deposited February 4, 2019.